On the Invisible Component of Massive Single Line Spectroscopic Binaries

Wiebke Riedel

Bachelorarbeit in Physik
angefertigt im Argelander-Institut für Astronomie

vorgelegt der
Mathematisch-Naturwissenschaftlichen Fakultät
der
Rheinischen Friedrich-Wilhelms-Universität
Bonn

Juni 2018

Ich versichere, dass ich diese Arbeit selbstständig verfasst und keine anderen als die angegebenen Quellen und Hilfsmittel benutzt sowie die Zitate kenntlich gemacht habe.

Bonn, ...

Datum Unterschrift

1. Gutachter: Prof. Dr. Norbert Langer
2. Gutachter: Prof. Dr. Thomas Tauris

Contents

CHAPTER 1

Introduction

In the course of the last few decades, it has become increasingly clear that a large fraction of stars - up to half of them - are located in stellar binary systems [1, p. 179]. An important point in understanding the significance of the large binary ratio among massive stars is the fact that they are known to terminate their life by graviational collapse, in which they form massive compact objects such as neutron stars or black holes. These objects represent particularly interesting forms of stellar endproducts, which could help to test the theories of gravity and many-body physics.

As interesting as this extraordinary compactness is, it is also the main challenge in the quest to find such objects. Even stellar black holes with relatively high masses have, astrophysically speaking, very small sizes. The Schwarzschild radius of a stellar black hole lies typically in the order of a few kilometers. It is therefore not possible to detect a stellar black hole directly. One has to rely on indirect methods.

In the past four decades, many discoveries of stellar mass black holes in single-line spectroscopic binary systems were made. Single line spectroscopic binaries (SB1) are binaries for which it is only possible to observe one stellar spectrum, but which also show a significant variation of their radial velocity curves. Most of them were discovered because their systems are extraordinarily luminous X-ray sources with a very short timescale variability up to the millisecond regime, which suggests a binary model where X-rays are emitted due to accretion of matter onto a compact object [2]. This kind of model requires a close, interacting binary, as it is necessary to have a significant amount of accretable matter. This matter is commonly provided from the stellar binary partner by stellar winds or even by Roche-lobe overflow. But there are also massive binary systems in which the stars are not close enough for this sort of accretion and therefore show no elevated X-ray flux when the system contains a stellar black hole.

This thesis aims to develop methods, that can help to find such systems. It attempts to develop methods to determine the lower and upper mass-limits of an invisible companion in a wide SB1-system, where it is possible to treat the stars as two single-stars. For this purpose, we use different approaches. To constrain the mass of the invisible star, the recorded stellar spectrum of the visible star is evaluated and the mass function $f(M)$, which can provide a lower mass limit, is calculated. An upper mass limit is determined by comparing the fluxes of both stars and calculating the smallest mass ratio for which the flux ratio can be measured. Finally, it is possible to constrain a lower mass limit for the initial mass of the invisible star, due to the fact that both of the stars have the same age.

In addition, one aim of the thesis is to determine stellar parameters which promise high masses of the invisible companion to simplify the search for promising SB1-systems. Finally, the methods that were developed in chapter 3 are applied to a selection of such SB1-systems.

CHAPTER 2

Theoretical Background

The objects of investigation in this thesis are single line spectroscopic binary systems (short: SB1). They consist of a visible star and an invisible companion, for which it is not possible to record a spectrum. In the following, the visible star is designated by first or primary star and the invisible one as second star. All physical quantities which are solely related to the visible star receive the index 1, all quantities which are solely related to the invisible star receive the index 2. For example M_1, L_1 and τ_1 are the mass, the luminosity and the lifetime of the visible star, M_2, L_2 and τ_2 are the mass, the luminosity and the lifetime of the invisible star.

2.1 The Mass Function

[1] Single line spectroscopic binaries are stellar binary systems for which it is only possible to observe the stellar spectrum of one of the stars. The spectrum of the companion is not visible, because the object is much fainter than the primary star.
The only evidence for the existence of an invisible companion in a stellar binary system is the Doppler shift of the line positions in the spectrum of the more luminous star, due to the periodic motion of both stars around their mutual barycentre. The frequency ν', observed in the moving frame, is related through the following equation to the frequency ν at rest and the radial velocity v_{rad} of the first star:

$$\nu' = \nu \cdot \sqrt{\frac{c \pm v_{\mathrm{rad}}}{c \mp v_{\mathrm{rad}}}},$$

where c is the velocity of light.
If the spectrum measurements lasted a sufficiently long time span, it is possible to generate a velocity curve for the binary system. It shows the behaviour of the total radial velocity as a function of time.

Figure 2.1 illustrates the formation of the velocity curve for the simplest case of a circular orbit for both stars. The line of sight is chosen to be from bottom to top. In step a and c the radial velocity disappears and the tangential velocity reaches its maximum value. In constrast to that the tangential velocity disappears in step b and d, whereas the radial velocity reaches its maximum. More complicated

[1] This section is based upon Chapters 2 in 'An introduction to the evolution of single and binary stars' by Benacquista, M. [1] if not stated otherwise.

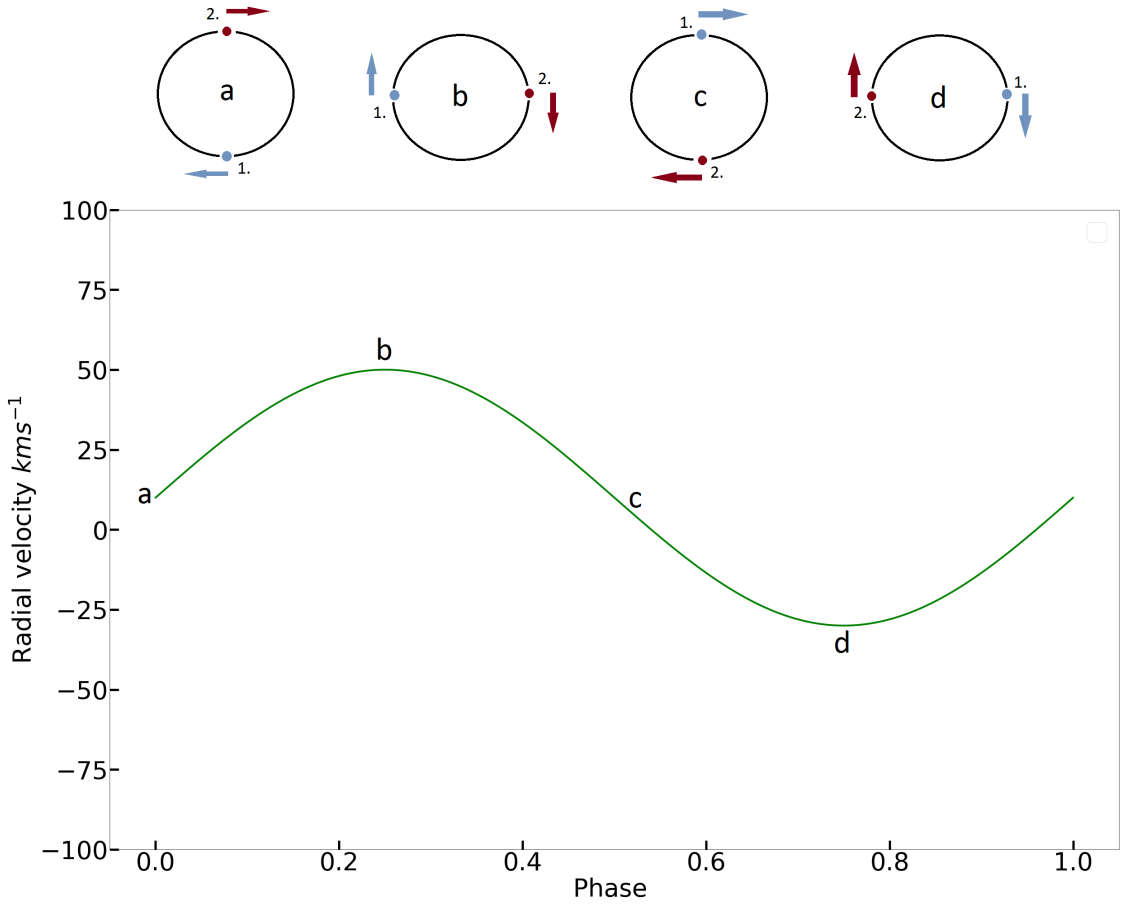

Figure 2.1: example of a radial velocity curve; step a and c $v_{\text{rad}} = 0 \implies v_{\text{tan}} = \max$, step b and d $v_{\text{tan}} = 0 \implies v_{\text{rad}} = \max$

examples can be seen in figure 2.2.

The shape of this curve depends on the radial velocity $\dot{z}$ and the systemic motion γ:

$$v_{\text{rad}} = \dot{z} + \gamma.$$

In general, the motion of both stars is located in two plain elliptical orbits for which the mutual barycentre of the system lies in one of the two foci of the ellipse. Due to this geometry, it is possible to describe the position of star i with polar coordinates r_i and θ_i.

The position of the star along the line of sight is a function of the inclination angle i, the longitude of the

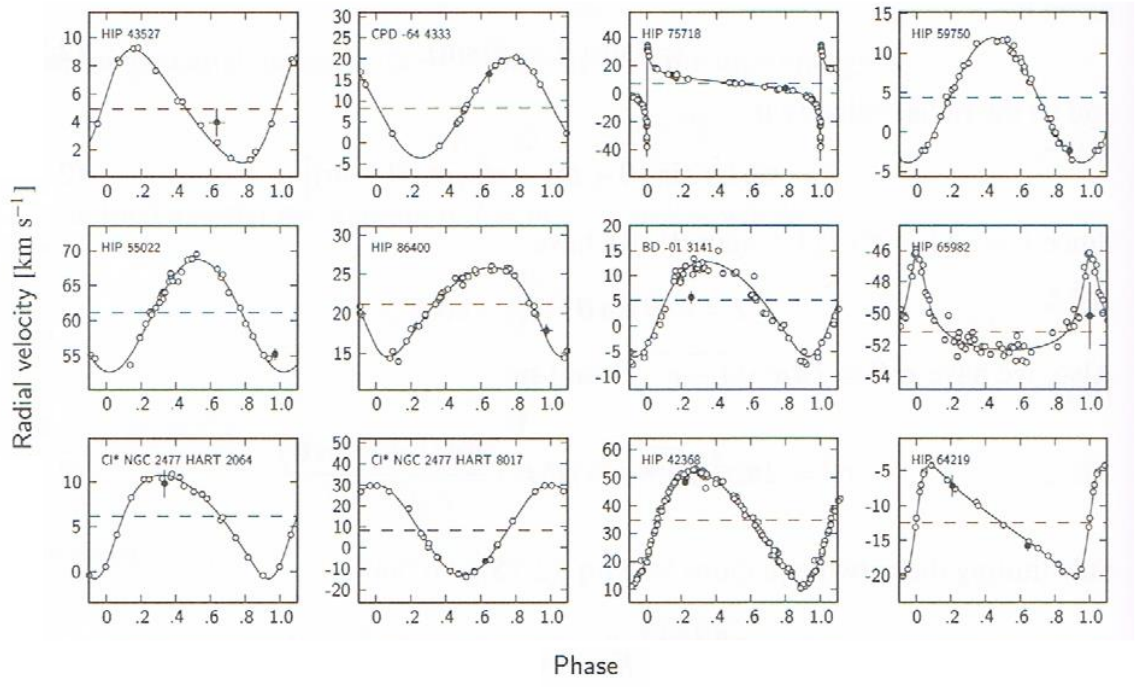

Figure 2.2: example for radial velocity curves of SB1-systems, figure taken from [1, S. 26]

periastron ω and the polar coordinate θ, as can be seen with the help of figure 2.3:

$$z = r sin(\theta + \omega) sin(i).$$

With a derivative with respect to time it is possible to express the radial velocity $\dot{z}$ in terms of these quantities:

$$\dot{z} = sin(i)(\dot{r} sin(\theta + \omega) + r\dot{\theta} cos(\theta + \omega)). \tag{2.1}$$

For this equation to be more useful, one can substitute $\dot{r}$ and $r\dot{\theta}$ by more pictorial quantities of ellipse, which can be done by substituting 2.2 and 2.3 into 2.1, whereby the new quantities a - the semimajor axis-, e -the eccentricity- and P -the orbital period- are introduced.

$$\dot{r} = \frac{2\pi a}{P} \frac{e sin(\theta)}{(1 + e cos(\theta))} \frac{(1 + e cos(\theta))}{\sqrt{1 - e^2}} \tag{2.2}$$

$$r\dot{\theta} = \frac{2\pi a (1 + e cos(\theta))}{P\sqrt{1 - e^2}} \tag{2.3}$$

$$\implies \dot{z} = sin(i) \frac{2\pi a}{P\sqrt{1 - e^2}} (e sin(\theta) sin(\theta + \omega) + e cos(\theta) cos(\theta + \omega) + cos(\theta + \omega))$$

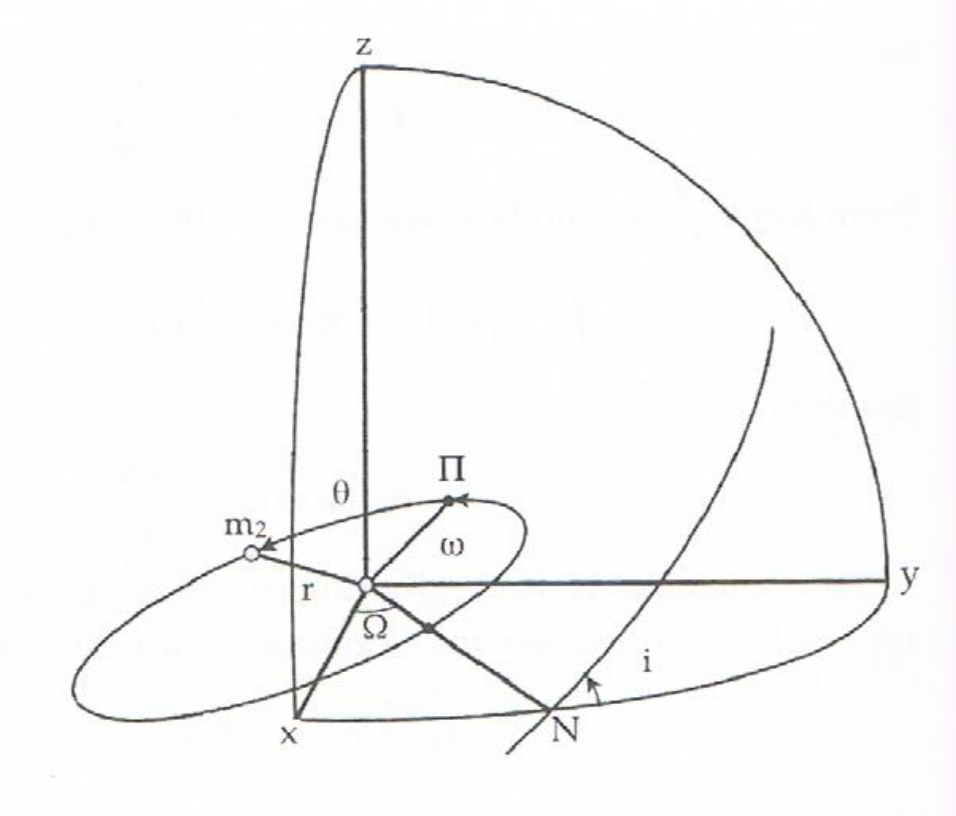

Figure 2.3: orbital elements of a SB1-systems, figure taken from [1, S. 22]

With the trigonometric relation $cos(x \pm y) = cos(x)cos(y) \mp sin(x)sin(y)$, one can simplify this equation.

$$\dot{z} = sin(i)\frac{2\pi a}{P\sqrt{1-e^2}}(ecos(\omega) + cos(\theta + \omega))$$

Therefore, the total radial velocity v_{rad} yields:

$$v_{\text{rad}} = K(ecos(\omega) + cos(\theta + \omega)) + \gamma. \tag{2.4}$$

With some small calculations one can show that K is the semi-amplitude of the velocity

$$\begin{aligned} \theta + \omega = 0 &\implies v_{max} = K(ecos(\omega) + 1) + \gamma \\ \theta + \omega = \pi &\implies v_{min} = K(ecos(\omega) - 1) + \gamma \end{aligned}$$

$$\begin{aligned} v_{max} - v_{min} &= Kecos(\theta) + K + \gamma - Kecos(\omega) + K - \gamma = 2K \\ K &= \frac{1}{2}(v_{max} - v_{min}) \end{aligned}$$

Therefore, one can obtain the values of the semi-amplitude of the velocity K_i, the eccentricity e, the longitude of the periastron ω and the systemic motion γ by fitting 2.4 to the shape of the measured velocity curve.

For a single-lined spectroscopic binary, one can only determine the semi-amplitude of the velocity for the first star K_1, for which the stellar spectrum is visible. With that information, it is possible to determine the value of the semimajor axis a_1 of the orbit of the visible star to a factor $sin(i)$. In general it is not possible to measure the inclination angle i.

$$K_1 = \frac{2\pi a_1 sin(i)}{P\sqrt{1-e^2}} \implies a_1 sin(i) = \frac{\sqrt{1-e^2}K_1 P}{2\pi} \tag{2.5}$$

Naturally, the semi-amplitude of the velocity of the second star K_2 is defined analogously:

$$K_2 = \frac{2\pi a_2 sin(i)}{P\sqrt{1-e^2}} \implies a_2 sin(i) = \frac{\sqrt{1-e^2}K_1 P}{2\pi} \tag{2.6}$$

With the relation $M_1 a_1 = M_2 a_2 \implies M_1 = M_2 \frac{a_2}{a_1}$, one can obtain an expression for the stellar masses M_1 and M_2 in terms of the the semi-amplitudes of the velocities K_1 and K_2:

$$M_1 = M_2 \left(\frac{a_2 sin(i)}{a_1 sin(i)}\right) = M_2 \frac{K_2}{K_1}. \tag{2.7}$$

With the use of Kepler's third law $GM = \frac{4\pi^2 a^3}{P^2}$, one obtains:

$$G(M_2 + M_1) = \frac{4\pi^2}{P^2}\left(\frac{a_1 sin(i) + a_2 sin(i)}{sin(i)}\right)^3$$

One can eliminate the quantities $a_1 sin(i)$, $a_2 sin(i)$ and M_1 using the relations 2.5, 2.6 and 2.7.

$$GM_2\left(\frac{K_1 + K_2}{K_1}\right) = \frac{4\pi^2}{P^2}\left(\frac{\sqrt{1-e^2}P}{2\pi}\right)^3 (K_1 + K_2)^3 \frac{1}{sin^3(i)}$$

After a transformation, the equation yields an expression for the mass M_2 of the invisible object.

$$M_2 sin^3(i) = \frac{P}{2\pi G}(1-e^2)^{3/2}(K_1 + K_2)^2 K_1$$

Because the spectrum of the second star is not visible and therefore K_2, the semi-amplitude of the velocity of star 2, is not measurable, one has to resubstitute it with the relation: $K_2 = \frac{M_1}{M_2}K_1$.

$$\begin{aligned} M_2 sin^3(i) &= \frac{P}{2\pi G}(1-e^2)^{3/2}\left(\frac{M_1 + M_2}{M_2}\right)^2 K_1^3 \\ f(m) &= \frac{M_2^3 sin^3(i)}{(M_1 + M_2)^2} = \frac{PK_1^3}{2\pi G}(1-e^2)^{3/2} \end{aligned} \tag{2.8}$$

Equation 2.8, called mass-function, provides an expression for the mass of the invisible star in a SB1-system, where only one stellar spectrum is visible. The mass of the visible star M_1 can be estimated by an empirical relation between the spectral type of a star and its mass. The quantities P, K_1 and e can be determined by evaluating the recorded velocity curve. The inclination angle i can, in general, not be

measured. It is therefore only possible to determine a lower limit of the mass $M_{2,min}$, which is achieved by setting $i = 90^\circ \implies sin(i) = 1$. A lower inclination angle i would correspond to a higher mass.

CHAPTER 3

Methods

3.1 The Solution of the Mass Function

In order to obtain an estimation of the lower mass limit for the invisible star $M_{2,min}$ it is necessary to solve the following equation:

$$\frac{M_2^3}{(M_1+M_2)^2} = f(M_2) \implies M_2^3 - f(M_2)M_2^2 - 2f(M_2)M_1M_2 - f(M_2)M_1^2 = 0 \tag{3.1}$$

Equation 3.1 is a third degree polynomial. It has two imaginary and one real solution. Given that the

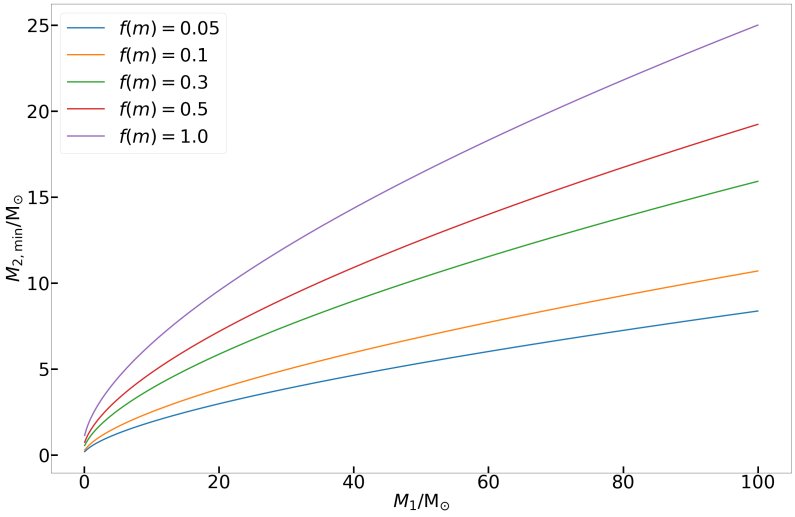

Figure 3.1: Real solution of equation 3.1 as a function of M_1 for different values of the mass-function $f(m)$

mass of the invisible star is a physical quantity, the real solution is the interesting one. The polynomial was solved with the calculation programme Mathematica. A visualisation of the real solution as a function of the mass of the first star for different typical values of the mass function $f(m)$ can be seen in figure 3.1.

$$M_{2,min} = \frac{f(M_2)}{3} - \frac{2^{1/3}(-f(M_2) - 6f(M_2)M_1)}{3C} + \frac{C}{3\cdot 2^{1/3}} \tag{3.2}$$

with:

$$C = \left(2f(M_2)^3 + 18f(M_2)^2 M_1 + 27f(M_2)M_1^2 + 3\sqrt{3}\sqrt{4f(M_2)^3 M_1^3 + 27f(M_2)^2 M_1^4}\right)^{1/3}.$$

3.2 The Flux Ratio of a Stellar Binary System

As seen in the previous chapter, the observed radial velocity curve provides a lower mass limit for the invisible second star of the binary. To further limit the possible mass interval, an upper limit would be desirable.
A possible way to find an upper limit for this mass is to find an expression of the flux ratio as a function of the mass ratio q of the two stars. One can then conclude for which mass ratio q it is still possible to measure the derived flux ratio. This mass ratio represents an upper limit q_{up} for the possible mass ratio range of the analysed SB1-system, due to the fact that the second star of the SB1-system is obviously not visible.

The flux ratio f_2/f_1 is defined as the flux which is emitted by the second star, compared to the flux of the first star. Due to the fact that both stars have, in very good approximation, the same distance to the observer, this ratio can also be expressed as a function of the intensities.

$$\frac{f_2}{f_1} = \frac{I(\nu, T_2)}{I(\nu, T_1)}\left(\frac{R_2}{R_1}\right)^2$$

It is assumed that Planck's law, which describes the specific intensity I_ν of a black-body for a given frequency ν and temperature T, is a good approximation for a stellar spectrum.
This specific intensity is given by: [3, p. 112]

$$I(\nu, T) = \frac{2h\nu^3}{c^2} \cdot \frac{1}{exp\left(\frac{h\nu}{k_B T}\right) - 1}.$$

Consequently, the ratio of intensities yields:

$$\frac{I(\nu, T_2)}{I(\nu, T_1)} = \frac{exp\left(\frac{h\nu}{k_B T_2}\right) - 1}{exp\left(\frac{h\nu}{k_B T_1}\right) - 1}.$$

The specific intensity I_ν is dictated by the effective temperatures T_{eff} of the two stellar components of the system. The surface temperature T_{eff} of a star depends on its radius R and its luminosity L. These physical quantities are connected via the Stefan-Boltzmann law: [3, p. 112]

$$T_{\text{eff}} = \sqrt[4]{\frac{L}{4\pi\sigma R^2}} \tag{3.3}$$

In order to express the flux ratio f_2/f_1 in terms of the mass-ratio q, it is therefore necessary to have a relation between mass and luminosity and also between mass and radius of a star.

This thesis uses an analytical expression obtained by Gräfener et al. [4] as mass-luminosity relation. They derived the dependence between mass and luminosity with the help of a grid for the mass

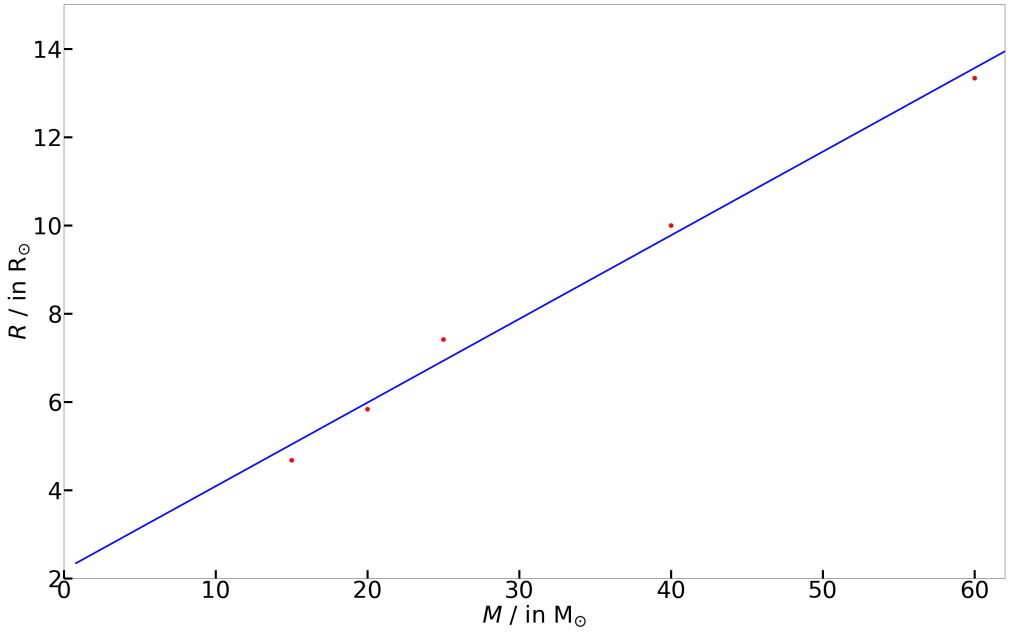

Figure 3.2: Linear function fitted on the converted intersections of 5 different evolution tracks with the isochrone at $10^{6.25} yrs$

range $M = 0.3 - 4000\,\mathrm{M}_\odot$ and hydrogen mass fractions $X_\mathrm{H} = 0.0 - 0.7$ at a solar metallicity.

Equation 3.4, which is quadratic in $\log(M)$ and linear in X_H, fits the results of $\log(L/\mathrm{L}_\odot)$ with a minimal accuracy of 0.02 in the parameter range $M = 12 - 250\,\mathrm{M}_\odot$ and $X_H = 0.1 - 0.7$, and with a minimal accuracy of 0.05 in the parameter range $M = 2 - 100\,\mathrm{M}_\odot$ and $X_\mathrm{H} = 0.1 - 0.7$. The corresponding parameter can be seen in tables 3.1 and 3.2.

$$\log\left(\frac{L}{\mathrm{L}_\odot}\right) = [F_1 + F_2 X_\mathrm{H}] + [F_3 + F_4 X_H] \cdot \log\left(\frac{M}{\mathrm{M}_\odot}\right) + [F_5 + F_6 X_H] \cdot \log\left(\frac{M}{\mathrm{M}_\odot}\right)^2 \tag{3.4}$$

Table 3.1: Coefficients $F_1 - F_6$ for the parameter range $M = 2 - 100\,\mathrm{M}_\odot$ and $X_\mathrm{H} = 0.1 - 0.7$; maximum fitting error for $\log(L/\mathrm{L}_\odot) = 0.05$

F1	1.967
F2	-2.943
F3	3.755
F4	1.206
F5	-0.727
F6	-0.026

Table 3.2: coefficients $F_1 - F_6$ for the parameter range $M = 12 - 250\,\mathrm{M}_\odot$ and $X_\mathrm{H} = 0.1 - 0.7$; maximum fitting error for $\log(L/\mathrm{L}_\odot) = 0.02$

F1	2.875
F2	-3.966
F3	2.496
F4	2.652
F5	-0.310
F6	-0.511

A suitable relation between mass and radius for heavy stars was developed by using the theoretical HRD on page 25 of the paper by Walborn, N.R. et al. [5]. The five points where the evolution tracks of the $15\,\mathrm{M}_\odot$,$20\,\mathrm{M}_\odot$, $25\,\mathrm{M}_\odot$, $40\,\mathrm{M}_\odot$ and $60\,\mathrm{M}_\odot$ stars meet the isochrone at $10^{6.25}$yr were converted with the help of the Stefan-Boltzmann law 3.3 to yield the radii of these stars. The obtained values in combination

with the stellar masses were used to derive the linear mass-radius relation 3.5. The fit onto these data points can be seen in figure 3.2.

$$R = (0.19 \pm 0.06)\frac{\mathrm{R}_\odot}{\mathrm{M}_\odot} \cdot M + (2.19 \pm 0.18)\mathrm{R}_\odot \tag{3.5}$$

Figure 3.3 shows the flux ratio f_2/f_1 as a function of the mass-ratio q, which was obtained with the mass-luminosity relation by Gräfener et al. [4] and the fitted linear mass-radius relation. As expected,

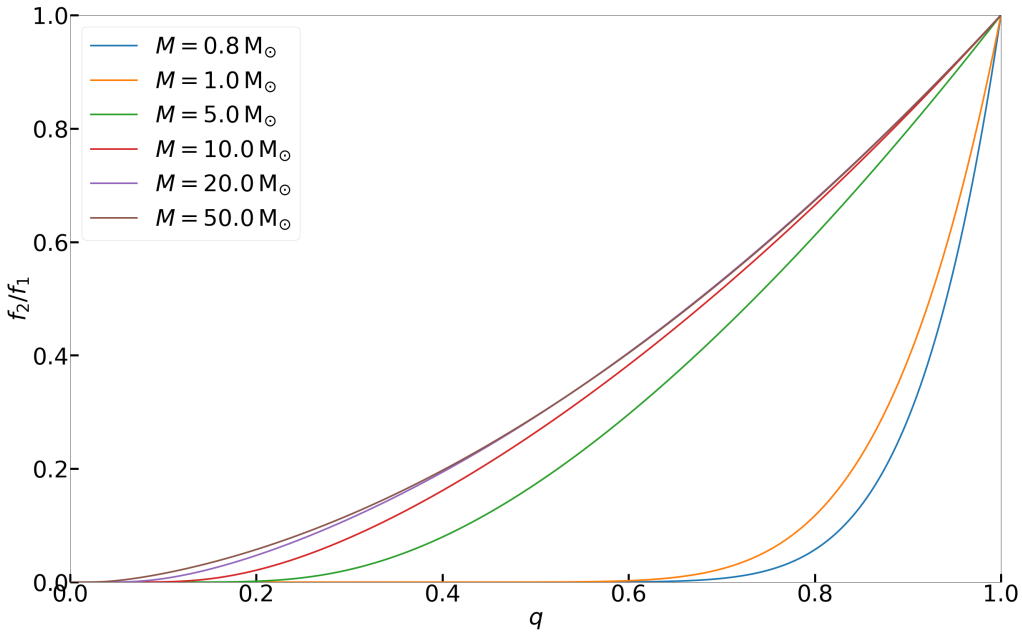

Figure 3.3: with mass-luminosity relation by Gräfener et al. [4] and fitted mass-radius relation calculated flux ratio f_2/f_1 as a function of mass ratio q, in a mass range of $0 \leq q \leq 1$, $\nu = 544$ THz/λ =550nm

the derived flux ratio is strongly dependent on the mass-ratio q of the SB1-system, the mass of the visible star M_1 and the frequency ν at which the observations are made. In figure 3.4, the range of the expected frequency variation in the visual realm of the electromagnetic spectrum can be seen.

Finally, it is necessary to transform the flux ratio into a magnitude ratio to compare these theoretical considerations with observational data. For historical reasons, magnitudes and intensities are connected through the following relation: [3, p. 183]

$$\Delta m = m_1 - m_2 = -2.5 \cdot \log\left(\frac{f_1}{f_2}\right)\mathrm{mag}$$

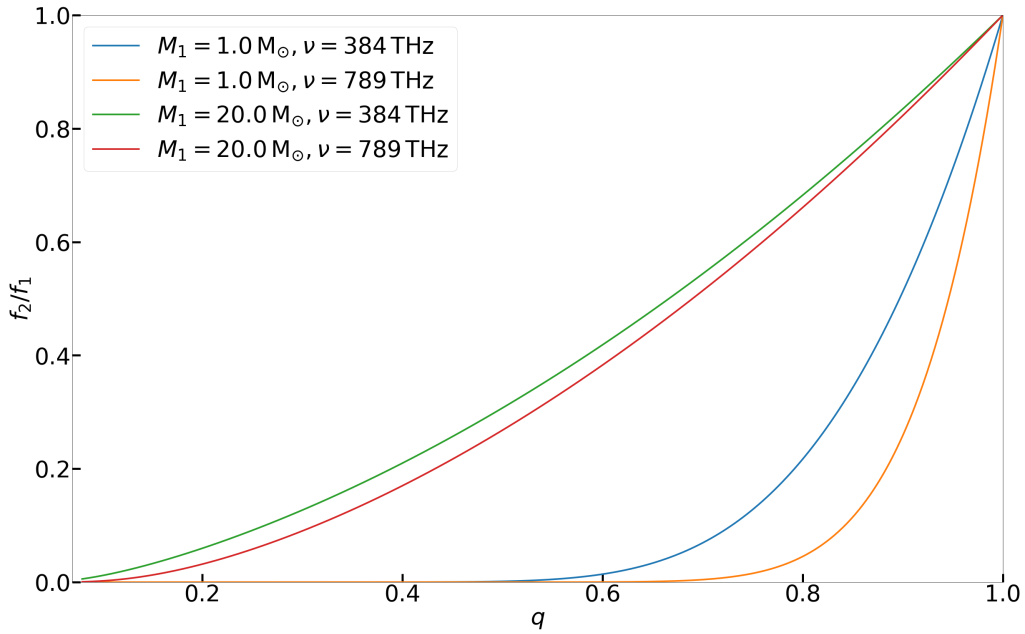

Figure 3.4: Flux ratio f_2/f_1 for the limiting frequencies of the visual realm for two different masses M_1

3.3 The Formation Time of a Stellar Binary System

Another approach to limit the possible mass interval of the invisible companion is to use the fact that both stars in the stellar binary system probably formed at roughly the same time and to use the correlation between the lifetime τ of a star and its mass M.

There are two possible reasons why the second star in a SB1-system is not visible. The first possibility is that both stars are main-sequence stars and the second star is too faint to be observable in close proximity to the much brighter visible first star. That would mean that the second star is less massive than the first star, which locates the binary system in the mass ratio range $0 \leq q \leq 1$.

The second possibility is that the mass of the second stars is higher than that of the first star, so that it has a shorter lifetime than the first star and could therefore already be in an endphase of stellar evolution. That would mean that the second star is more massive than the first star. For this second possibility one can derive a lower limit for the mass ratio range $1 \leq q$

The current time t, which has passed since the formation of the stellar binary system, can be expressed as fractional age d.

$$t = d \cdot \tau_1 \implies d = \frac{t}{\tau_1} \tag{3.6}$$

If the second star is already in its endstage of stellar evolution, its lifetime has to be shorter than or equal to the current time $t \geqq \tau_2$. This inequation can be used to derive a lower limit for the mass-ratio by examining the case $t = \tau_2$.

Using equation 3.6, this condition can be transformed to the following equation:

$$\tau_2 = d_{limit} \cdot \tau_1 \tag{3.7}$$

A relation between lifetime τ and mass M can be taken from the lecture notes by Pols, O.R. [6]: $\tau \propto M^{1-\eta}$, where the fact was used that the main sequence phase is by far the longest evolution phase for all considered stellar masses. Therefore, the lifetime of the first and the second star can be expressed as:

$$\tau_i = AM_i^{1-\eta}$$

A is assumed to be a constant coefficient. Inserting these relations in equation 3.7 yields:

$$AM_2^{1-\eta} = d_{limit} \cdot AM_1^{1-\eta}.$$

To eliminate the mass of the second star M_2, one substitutes it with the mass-ratio $q = \frac{M_2}{M_1} \implies M_2 = qM_1$.

$$Aq^{1-\eta}M_1^{1-\eta} = d_{limit} \cdot AM_1^{1-\eta}$$

Finally, one obtains an expression for the lower limit of the time fraction d_{limit} as a function of the mass ratio q:

$$d_{limit} = q^{1-\eta} \implies q = d_{limit}^{\frac{1}{1-\eta}} \tag{3.8}$$

Equation 3.8 represents a root function with a moderate decay. Due to the fact that a very simple approximation for the relation between luminosity L and mass M was assumed, equation 3.8 only provides a rough estimate on the form of the derived relation. To improve the quantitive description, a stellar grid for stars in the parameter range $M = 0.8 - 120\,M_\odot$ was used. It was calculated with a stellar evolution code by Georgy, C. et al. [7] for a metallicity of $Z = 0.002$ and by Ekström, S. et al. [8] for a metallicity of $Z = 0.014$. In this thesis, only stellar models without rotation are considered. In order to

Table 3.3: coefficients A, B and C for the parameter range $M = 0.8 - 120\,M_\odot$ and $Z = 0.002$

A	$4.0159\text{yr} \pm 0.0183\text{yr}$
B	$-0.3848\,M_\odot^{-1} \pm 0.0383\,M_\odot^{-1}$
C	$5.7030\text{yr} \pm 0.0136\text{yr}$

Table 3.4: coefficients A, B and C for the parameter range $M = 0.8 - 120\,M_\odot$ and $Z = 0.014$

A	$4.2709\text{yr} \pm 0.0210\text{yr}$
B	$-0.4028\,M_\odot^{-1} \pm 0.0450\,M_\odot^{-1}$
C	$5.7000\text{yr} \pm 0.0166\text{yr}$

calculate a similiar expression to relation 3.8, it is useful to be able to express the calculated correlation as a function. Function 3.9 was found to fit the 24 grid points sufficiently well.The first turn off point was used as the end of the main sequence, which is marked by track step 110. The resulting fitting parameter A, B and C and their errors are listed in table 3.3 for Z = 0.002 and in table 3.4 for Z = 0.014.

$$log(\tau_{MS}) = A \cdot 10^{B \cdot log(M)} + C \tag{3.9}$$

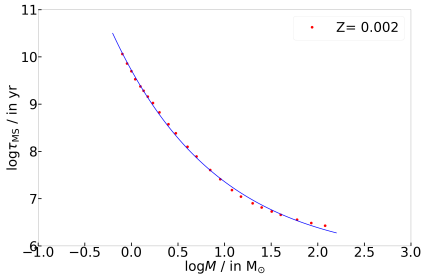

Figure 3.5: function 3.9 fitted on the stellar grid points, calculated by Georgy, C. et al. [7] for a metallicity of Z = 0.002

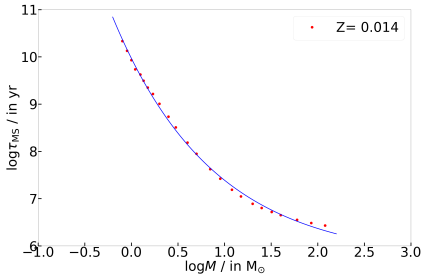

Figure 3.6: function 3.9 fitted on the stellar grid points, calculated by Ekström, S. et al. [8] for a metallicity of Z = 0.014

With the fitting function and the parameters that were obtained, one can derive an expression for the fractional age t/τ_1 as a function of the mass-ratio q, which can be seen by following the transformation steps leading to equation 3.11. Unfortunately, it is not possible to eliminate the mass of the first star M_1.

$$log(\tau_i) = A \cdot 10^{B \cdot log(M_i)} + C \implies \tau_i = 10^{A \cdot M_i^B + C} \tag{3.10}$$

$$10^{A \cdot M_2^B + C} = d_{limit} \cdot 10^{A \cdot M_1^B + C}$$
$$10^{A \cdot (qM_1)^B + C} = d_{limit} \cdot 10^{A \cdot M_1^B + C} \implies d_{limit} = 10^{A \cdot M_1^B (q^B - 1)} \tag{3.11}$$

equation 3.11 with the fitting parameter of Z = 0.002

$$d_{\text{limit}} = 10^{4.0159\text{yr} \cdot M_1^{-0.3848\,\text{M}_\odot^{-1}} (q^{-0.3848\,\text{M}_\odot^{-1}} - 1)} \tag{3.12}$$

equation 3.11 with the fitting parameter of Z = 0.014:

$$d_{limit} = 10^{4.2709\text{yr} \cdot M_1^{-0.4028\,\text{M}_\odot^{-1}} (q^{-0.4028\,\text{M}_\odot^{-1}} - 1)} \tag{3.13}$$

Therefore, the obtained relations 3.12 for the metallicity $Z = 0.002$ and 3.13 for the metallicity $Z = 0.014$ are plotted in figure 3.7 and in figure 3.8 for different masses of the first star M_1 (0.8 $M_\odot$, 1 $M_\odot$, 5 $M_\odot$, 10 $M_\odot$, 20 $M_\odot$, 50 $M_\odot$, 100 $M_\odot$). At this point, it is easy to see that the lower the mass of the first star M_1 is, the steeper is the decay of expression 3.12 and 3.13. For all plotted stellar masses, the function converges towards the x-axis.

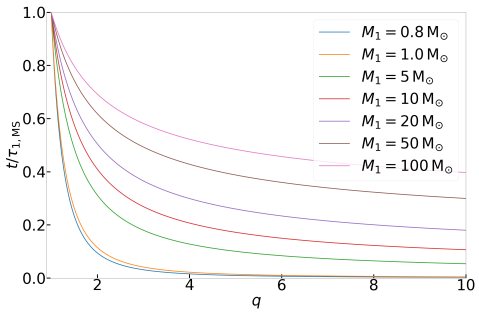

Figure 3.7: with the stellar grid calculated by Georgy, C. et al. [7], derived expression for the fractional t/τ_1 as a function of the mass-ratio q for different masses M_1

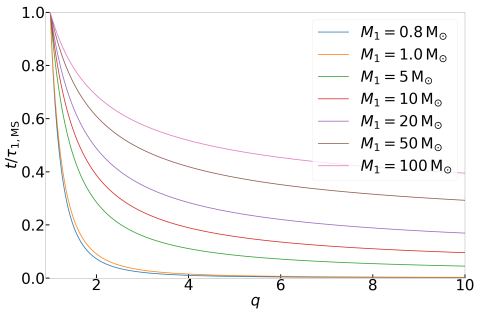

Figure 3.8: with the stellar grid calculated by Ekström, S. et al. [8], derived expression for the fractional t/τ_1 as a function of the mass-ratio q for different masses M_1

Additionally, the metallicity of the SB1-system has a small effect, which can be verified by a close look at figure 3.9. The relation for the smaller metallicity $Z = 0.002$ converges slightly more slowly towards the x-axis than the relation for the higher metallicity $Z = 0.014$.

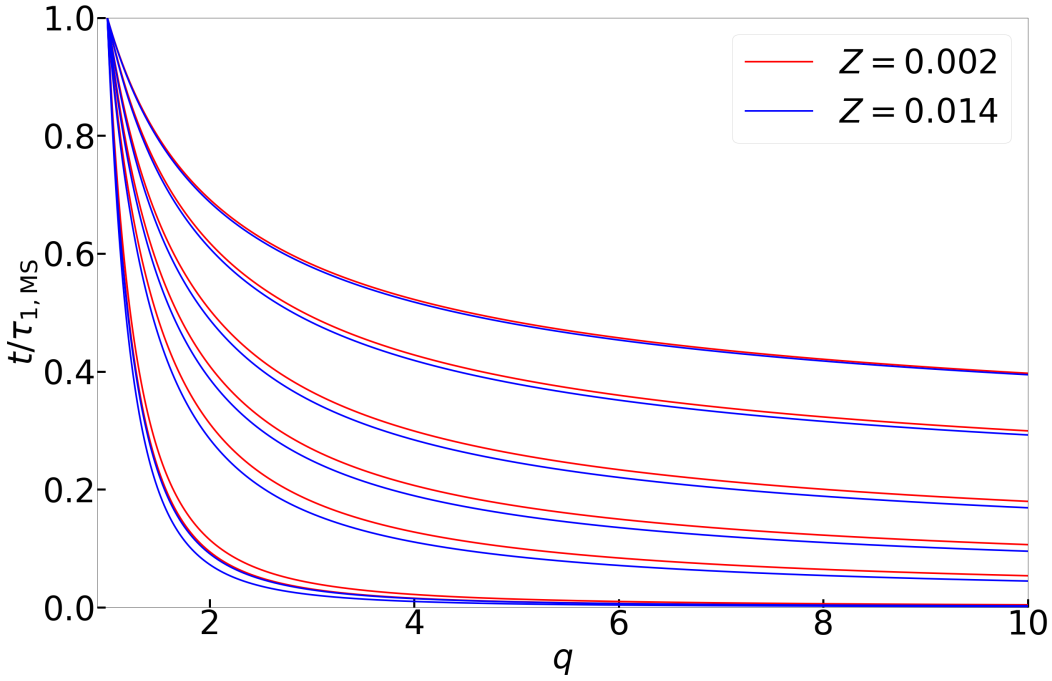

Figure 3.9: with the stellar grid by, calculated by Georgy, C. et al. [7] (for Z = 0.002) and Ekström, S. et al. [8] (for Z = 0.014), derived expression for the fractional age t/τ_1 as a function of the mass-ratio q for different masses M_1, comparision of the metallicities

By inverting relation 3.11, one can also derive a lower mass-limit $q_{\mathrm{min,time}}$ or a lower mass $M_{2,\mathrm{min,time}}$ for the second star for the case that it must be heavier than the visible star. Figure 3.10 and 3.11 illustrate that relation for Z=0.002 or respectively for Z=0.014. Before drawing that conclusion, one must exclude the

mass ratio-range $0 \leq q \leq 1$ for the SB1-system in question with the help of the two methods previously described.

$$q = \sqrt[B]{\frac{\log(d_{\text{limit}})}{AM_1^B} + 1} \tag{3.14}$$

The fractional age d can be expressed as:

$$d_{\text{limit}} = \frac{t}{\tau_1} = \frac{t}{10^{A \cdot M_1 + C}}$$

Equation 3.14 can therefore be transformed into:

$$q = \sqrt[B]{\frac{\log(t) - (AM_1^B + C)}{AM_1^B} + 1} \implies M_2 = \left(\sqrt[B]{\frac{\log(t) - (AM_1^B + C)}{AM_1^B} + 1} \right) M_1$$

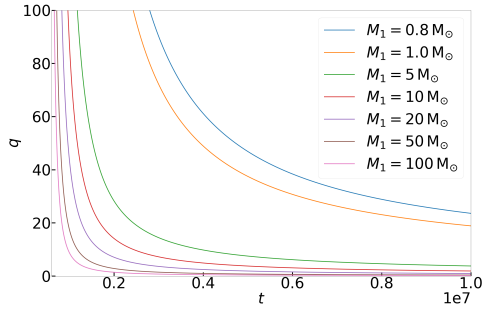

Figure 3.10: with the stellar grid calculated by Georgy, C. et al. [7], derived expression for the the mass-ratio q as a function of fractional t/τ_1 for different masses M_1

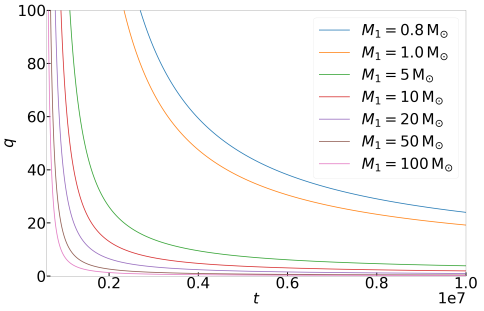

Figure 3.11: with the stellar grid calculated by Ekström, S. et al. [8], derived expression for the the mass-ratio q as a function of fractional t/τ_1 for different masses M_1

CHAPTER 4

Results

In order to apply the various methods developed in chapter 3, the observational data of two different papers was used.
In the paper by Williams, S.J. et al. [9], the orbits of five Galactic O-type stars with significant single-lined spectroscopic variation were published. The data comes from current measurements of the five systems at the Cerro Tololo Inter-American Oberservatory (CTIO) and the Kitt Peak National Oberservatory, but also from older measurements of the systems, which were collected from the literature.
The paper by Almeida L.A. et al. [10] lists the dynamical data from several O-type binary systems which were observed during the VLT-Flames Tarantula Survey. These include 51 single-line spectroscopic binary systems (SB1).

By fitting the observed velocity curves, the authors of both papers obtained values for the semiamplitude of the velocity K, the orbital period P and the eccentricity e, which are necessary to calculate a mass function f(M) using equation 2.8. These calculations were carried out in this thesis and can be seen in tables A.4 and A.5 in column (7).

To calculate a lower mass-limit for the invisible star $M_{2,\mathrm{min}}$, one has to determine the mass of the visible star M_1. For this purpose, the observed spectra are evaluated to obtain values for the effective temperature T_{eff}, the gravitational acceleration g and the rotational velocity $vsin(i)$ at the equator of the star, multiplied with the sine of the inclination angle i. Using these physical qunatities, it is possible to calculate other important quantities of the primary star such as its luminosity or its mass. Some of the luminosities of the primary stars of the SB1s, listed in Almeida L.A. et al. [10] are already calculated in a paper by Walborn N.R. et al. [5]. Unfortunately, this data could only be determined for 33 of the systems. Therefore the analysis could just be done for these 33 systems. An estimation of the error bars is not given, which is why a propagation of uncertainty was omitted.

This data was used to further determine the mass and other useful physical quantities of the visible star by using the stellar evolution code "BONNSAI[1] (Schneider et al. 2014)". The obtained data is listed in table A.3.

In addition, we used equation 3.2 to calculate the lower mass limit $M_{2,\mathrm{min}}$ of the invisible star and the resulting lower limit for the mass ratio q_{min}. The results of this calculation can be seen in column (8) and (9) of tables A.4 and A.5.

For the calculation of the optical characteristics of the systems, we assumed a hydrogen mass fraction

[1] The BONNSAI web-service is available at www.astro.uni-bonn.de/stars/bonnsai.

Table 4.1: comparision of flux ratio and magnitude differences at the most probable mass ratio q_{prop} between the results of Williams, S.J. et al [9] (index $_{\text{Wil.}}$) and the results of this thesis (index $_{\text{T}}$)

system	q_{prob}	$\frac{I_2}{I_1}(q_{\text{prob}})_{\text{Wil.}}$	$\Delta V_{\text{Wil.}}$/mag	$\frac{I_2}{I_1}(q_{\text{prob}})_{\text{T}}$	ΔV_{T}/mag
HDE 308813	0.26	0.08	2.7	0.07	2.9
HD 152147	0.18	0.01	4.8	0.07	2.9
HD 164536	0.30	0.12	2.3	0.12	2.3
BD-16°4826	0.19	0.06	3.1	0.05	3.3
HDE 229232	0.16	0.05	3.2	0.03	3.6

X_H of 0.7. Moreover, we chose the midpoint of the V-Filter at $544THz(\widehat{=}550nm)$ as analysing frequency. In contrast to the calculations for the lower mass limit, where we used the actual mass, the initial mass of the first star M_{ini} was used, as the mass-radius relation was fitted using the initial mass of the star. We also used the observed effective temperature T_{eff} for the description of the blackbody-spectrum of the first star. Only the resulting upper mass limit q_{up} was then calculated with the actual mass M_{act} of the primary star. Both masses were determined with "BONNSAI" and are also listed in table A.3 in columns (3) and (4).

To test the results of the flux ratio and magnitude difference, we calculated these physical quantities for the five systems presented in the paper by Williams, S.J. et al. [9], at the mass ratio which they determined as propable mass ratio q_{prop}. They assumed a uniform mass ratio distribution, which is motivated by observation of O-type stars . The authors of the paper by Williams, S.J. et al. [9] used listed values from the book "The Observation and Analysis of Stellar Photospheres" by Gray, D. F. [11] to determine flux ratio and magnitude difference. The comparision can be seen in table 4.1. The results from both methods are in relatively good agreement with each other. Solely for system HD 152147, the results differ slightly more. However, the knowledge of the flux ratio and the magnitude difference at the most probable mass ratio q_{prop} is not useful, in particular if the used mass ratio distribution is flat. Therefore this thesis takes an other approach.

The results of the calculations can be seen in tables A.4 and A.4. In columns (10) and (11) the flux ratio f_2/f_1 and the magnitude difference Δm respectively, at q_{min} are determined to check how sensitive a measurement would have to be to give a complete constraint on the mass of the invisible star. Columns (12), (13) and (14) list values of the mass ratio q_{up} for the different flux ratios f_2/f_1 0.1, 0.2 and 0.3, which symbolise different sensitivity limits of the measurements and should give an idea to which extent an improvement of the accuracy of the measurements could improve the constraints on the determined mass-intervals. To obtain these limits for q_{up}, the function for the flux ratio f_2/f_1 , which was developed in chapter 3.2, was numerically inverted.

It may also prove useful to sort the analysed systems into different groups according to the likelihood that the mass range of $0 \leq q \leq 1$ can be excluded for the system. With the help of this sorting mechanism, we introduced four different groups. Group 1 consists of systems where $q_{\text{up10\%}}$ is above q_{min}, making it highly unlikely that the flux ratio can be measured accurately enough to give a complete constraint on the mass of the second star M_2. Group 2 and group 3 comprise systems where q_{min} lies between $q_{\text{up10\%}}$ and $q_{\text{up20\%}}$, and between $q_{\text{up20\%}}$ and $q_{\text{up30\%}}$ respectively. Group 4 consist of systems where q_{min} lies above $q_{\text{up30\%}}$. At least for the systems in group 4, one can expect that the mass range of $0 \leq q \leq 1$ can be excluded.

For systems fulfilling this criterion, the third developed method can raise the lower mass limit. In columns (15) and (16) of tables A.4 and A.4, the constraints for the initial mass of the second star, due to

fact that the systems formed roughly at the same time, are given.

Some of the analysed systems are quite young and can therefore not contain a star which has already terminated its stellar evolution. For this reason, some of the calculated values are unreasonably high. A mass range of $q \geq 1$ can therefore be excluded for these systems.

Given the approximations that were made to develop the used methods, and the hence resulting inaccuracy, the calculated constraints may be more interesting for members of groups 3 and 4.

CHAPTER 5

Conclusions

The SB1 systems analysed in the paper by Almeida L.A. et al. [10] proved to be excellent candidates for the applied evaluation process, as almost all of them show long orbital periods P and high semi-amplitudes of the velocity K_1. Hence the systems have a high mass function $f(m)$ and consequently a relatively high lower mass ratio q_{low}. This circumstance makes it more unlikely that the second star could be overlooked. All of the members of group 2 to 4 are from this paper by Almeida L.A. [10]. Most of them have orbital periods P in the order of a few hundred days. This fact is invidious, because it means that such promising candidates can only be detected with observations over a long time span, which poses a large effort.

Unfortunately, the five systems analysed in the paper by Williams, S.J. et al.[9] are not as suitable as the others. They have relatively short orbital periods of just a few days, which is obviously too small to produce a high mass function $f(m)$. Consequently, they have relatively small lower mass limits q_{low}, which is probably why it is not possible to see the second star. All of them are sorted into group 1.

It also emerged that massive primaries are better candidates for this kind of analysis. The flux ratio ratio f_2/f_1 converges faster to a value of 1.0. Therefore, the upper mass limits $q_{\mathrm{up,i\%}}$ are lower than for less massive stars.

In the course of the development of the flux ratio q_{up}, it became clear that particularly the mass-radius relation has a strong influence on the calculated flux ratio. In this thesis, a mass-radius relation was used that is a good description for stars of the age $10^{6.25}$yrs. Obviously, this relation becomes more and more inaccurate with increasing age of the system. For this reason, it would be a good improvement of the used methods to consider the evolutionary changes of the important physical quantities effective temperature T_{eff}, luminosity L and radius R. Especially the increase of the stellar radius along the main sequence should be taken into account.

To provide a self-consistent evaluation the mass-radius relation was used for both stars. Even if the "BONNSAI" values differ from that, which they do especially for the older systems, the effect is not very significant, because it partly cancels itself out, due to the fact that we calculate the quadratic fraction of the radii. However as a consequence, the determined flux ratio is systematically slightly too high for the older systems.

As expected, it was possible with the help of the third method to determine a lower limit of the initial mass, which is significantly higher than the lower mass limit calculated by means of the mass function. Adequate models that describe the possible mass loss up to the invidual actual age of the analysed systems could therefore provide a higher lower mass limit for the actual mass than the observations of the radial velocity curve, if it is possible to exclude the mass ratio range of $0 \leq q \leq 1$.

At this point, the analysed systems can be sorted into the introduced groups and their possible mass

range can be visualised, which is done in figures 5.1, 5.2 and 5.3.

Most of the systems are sorted into group 1, which matches our expectations. There are eight systems in group 2 for which it might be possible to record a second spectrum with more accurate observations. These systems are not necessarily compact objects.

Group 3 merely consists of the system 429, and group 4 consists of the systems 064, 332 and 802. For these systems, it would most likely be possible to detect the second star, if it were a star on the main sequence. It is therefore likely that these partners are in fact compact objects, more precisely stellar black holes, because they are too heavy for neutron stars.

These four systems are pretty interesting for physicists, seeing that they probably consist of a black hole and a visible star, that will also terminate its life by forming a black hole. Such relatively close black holes are likely to merge. A merger of massive stellar black holes produces gravitational waves, which could be measured by LIGO.

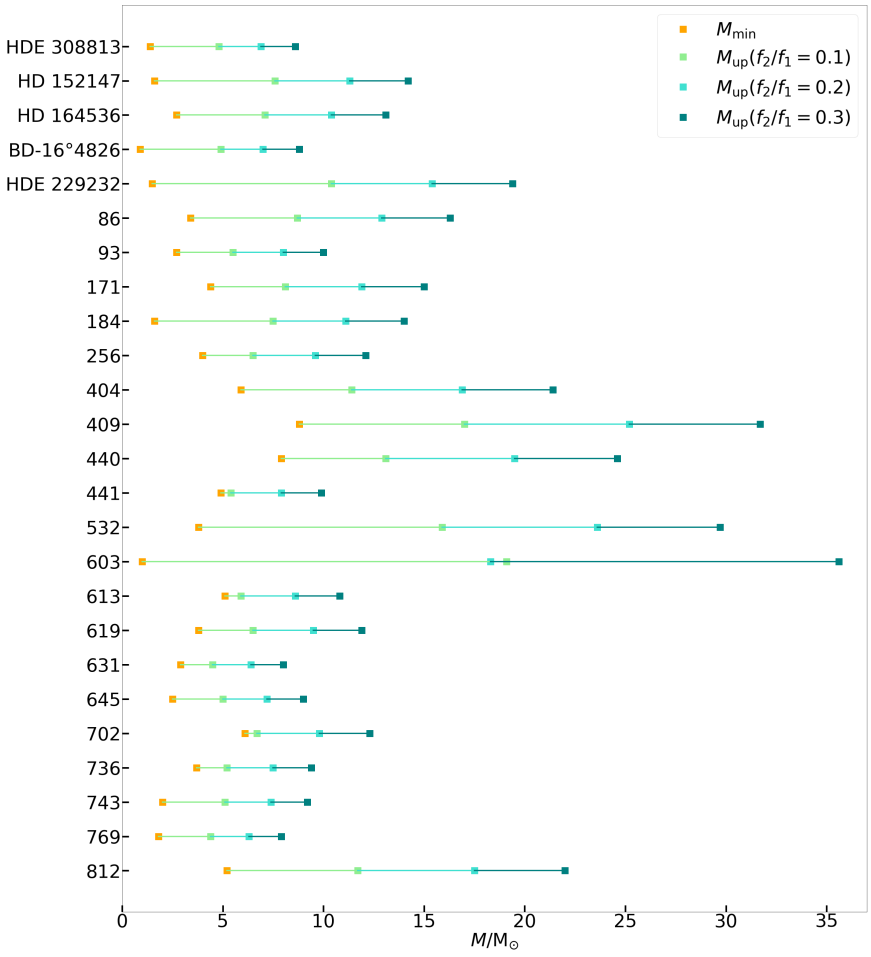

Figure 5.1: possible mass-intervals for group 1, which is defined by $q_{\min} < q_{\mathrm{up10\%}}$

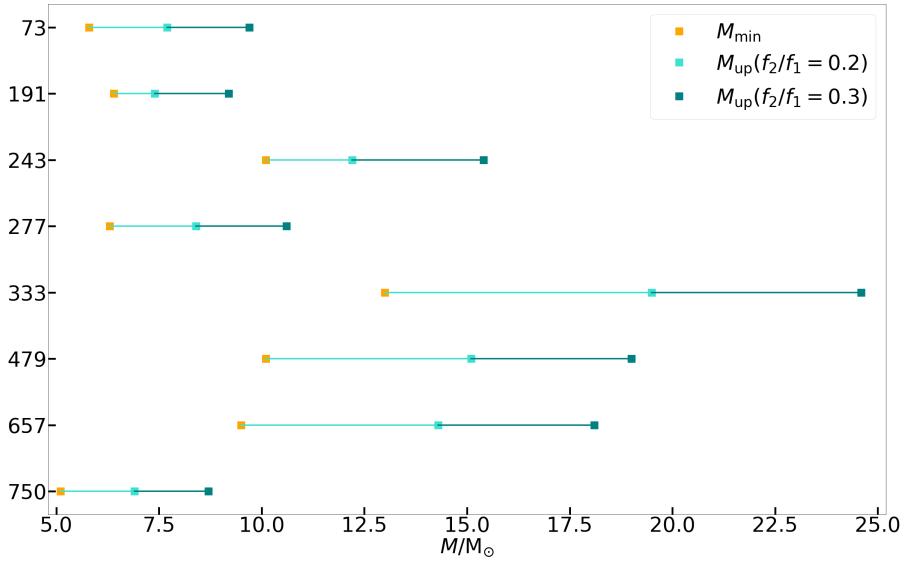

Figure 5.2: possible mass-intervals for group 2, which is defined by $q_{\text{up10\%}} < q_{\text{min}} < q_{\text{up20\%}}$

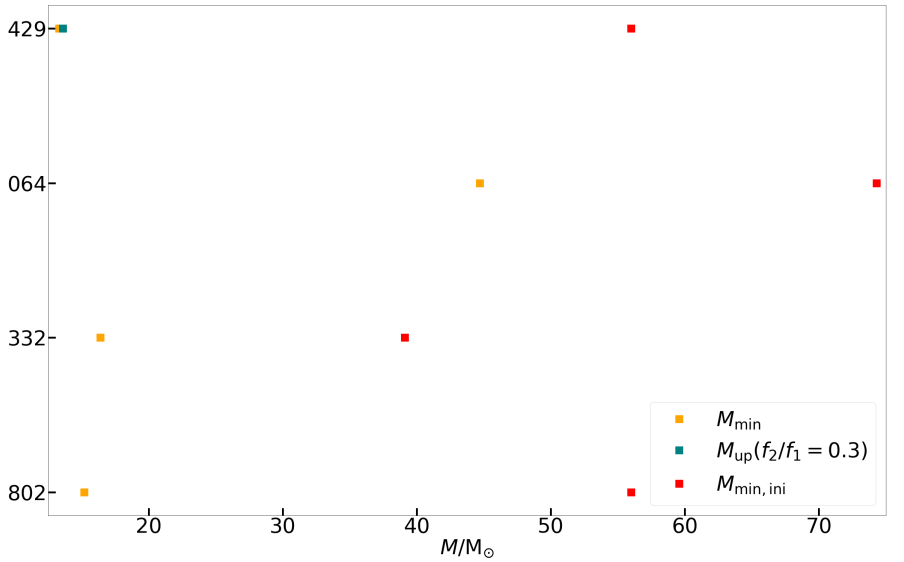

Figure 5.3: possible mass-intervals for group 3, which is defined by $q_{up20\%} < q_{min} < q_{up30\%}$ and possible mass-intervals for group 4, which is defined by $q_{\text{min}} > q_{\text{up30\%}}$

Bibliography

[1] M. Benacquista, *An introduction to the evolution of single and binary stars*, Springer Science & Business Media, 2012 (cit. on pp. 1, 3, 5, 6).

[2] J. Casares, *Observational evidence for stellar-mass black holes*, Proceedings of the International Astronomical Union **2** (2006) 3 (cit. on p. 1).

[3] A. Unsöld and B. Baschek, *Der neue Kosmos, 7. Aufl. Korrigierter Nachdruck*, (2005) (cit. on pp. 10, 12).

[4] G. Gräfener et al., *The Eddington factor as the key to understand the winds of the most massive stars-Evidence for a* Γ*-dependence of Wolf-Rayet type mass loss*, Astronomy & Astrophysics **535** (2011) A56 (cit. on pp. 10, 12).

[5] N. Walborn et al., *The VLT-FLAMES Tarantula Survey-XIV. The O-type stellar content of 30 Doradus*, Astronomy & Astrophysics **564** (2014) A40 (cit. on pp. 11, 19).

[6] O. Pols, *Stellar Structure and Evolution*, 2009 (cit. on p. 14).

[7] C. Georgy et al., *Grids of stellar models with rotation-III. Models from 0.8 to 120 M at a metallicity Z= 0.002*, Astronomy & Astrophysics **558** (2013) A103 (cit. on pp. 14–17).

[8] S. Ekström et al., *Grids of stellar models with rotation-I. Models from 0.8 to 120 M at solar metallicity (Z= 0.014)*, Astronomy & Astrophysics **537** (2012) A146 (cit. on pp. 14–17).

[9] S. Williams et al., *Radial Velocities of Galactic O-Type Stars. II. Single-lined Spectroscopic Binaries*, The Astronomical Journal **145** (2012) 29 (cit. on pp. 19, 20, 23).

[10] L. Almeida et al., *The Tarantula Massive Binary Monitoring-I. Observational campaign and OB-type spectroscopic binaries*, Astronomy & Astrophysics **598** (2017) A84 (cit. on pp. 19, 23).

[11] D. F. Gray, *The observation and analysis of stellar photospheres*, Cambridge University Press, 2005 (cit. on p. 20).

APPENDIX A

Tables

Table A.1: the stellar grid points, calculated by Georgy, C. et al [7] for a metallicity of Z = 0.002

step	initial mass	time	current mass	$log(L)$	$log(T_{\text{eff}})$
110	0.80	1.14964e+10	0.80	0.158	3.787
110	0.90	7.25017e+09	0.90	0.338	3.805
110	1.00	4.98845e+09	1.00	0.514	3.835
110	1.10	3.37235e+09	1.10	0.648	3.862
110	1.25	2.36210e+09	1.25	0.852	3.903
110	1.35	1.92228e+09	1.35	1.011	3.931
110	1.50	1.44475e+09	1.50	1.205	3.964
110	1.70	1.06116e+09	1.70	1.453	4.003
110	2.00	6.72549e+08	2.00	1.727	4.047
110	2.50	3.77285e+08	2.50	2.098	4.105
110	3.00	2.42421e+08	3.00	2.392	4.151
110	4.00	1.25522e+08	4.00	2.838	4.224
110	5.00	7.80867e+07	5.00	3.176	4.277
110	7.00	4.03362e+07	7.00	3.668	4.351
110	9.00	2.57252e+07	9.00	4.021	4.401
110	12.00	1.52435e+07	11.97	4.404	4.452
110	15.00	1.10999e+07	14.92	4.685	4.486
110	20.00	7.95762e+06	19.91	5.024	4.525
110	25.00	6.50584e+06	24.78	5.261	4.547
110	32.00	5.33918e+06	31.51	5.497	4.563
110	40.00	4.54429e+06	39.10	5.686	4.571
110	60.00	3.58240e+06	57.79	5.991	4.559
110	85.00	3.04612e+06	80.91	6.221	4.514
110	120.00	2.67199e+06	111.75	6.429	4.345

Table A.2: stellar grid points, calculated by Ekström, S. et al [8] for a metallicity of Z = 0.014

step	initial mass	time	current mass	$log(L)$	$log(T_{\text{eff}})$
110	0.80	2.15078e+10	0.80	-0.207	3.715
110	0.90	1.34162e+10	0.90	-0.009	3.741
110	1.00	8.49545e+09	1.00	0.157	3.762
110	1.10	5.46053e+09	1.10	0.305	3.780
110	1.25	4.22249e+09	1.25	0.582	3.800
110	1.35	3.13865e+09	1.35	0.738	3.817
110	1.50	2.23918e+09	1.50	0.938	3.839
110	1.70	1.64515e+09	1.70	1.189	3.864
110	2.00	1.01704e+09	2.00	1.484	3.912
110	2.50	5.42325e+08	2.50	1.883	3.978
110	3.00	3.23213e+08	3.00	2.198	4.036
110	4.00	1.53435e+08	4.00	2.686	4.123
110	5.00	8.89959e+07	5.00	3.052	4.188
110	7.00	4.21159e+07	7.00	3.583	4.279
110	9.00	2.65086e+07	8.99	3.965	4.338
110	12.00	1.54981e+07	11.94	4.366	4.396
110	15.00	1.11333e+07	14.81	4.654	4.431
110	20.00	7.81899e+06	19.67	5.001	4.467
110	25.00	6.37078e+06	24.18	5.235	4.480
110	32.00	5.25168e+06	30.11	5.460	4.476
110	40.00	4.47708e+06	36.26	5.642	4.452
110	60.00	3.55952e+06	36.261	5.910	4.412
110	85.00	3.04802e+06	49.232	6.146	4.517
110	120.00	2.69160e+06	63.625	6.348	4.433

Table A.3: by BONNSAI calculated physical quantities of the primary stars compared to the oberved quantities

system		HDE 308813	HD 152147	HD 164536	BD-16°4826	HDE 229232
$T_{eff,obs}$ /kK	(1)	29.9 ± 0.3	27.8 ± 0.5	37.4 ± 0.9	39.9 ± 6.3	41.7 ± 1.3
$T_{eff,rep}$ /kK	(2)	29861^{+323}_{-289}	27784^{+495}_{-529}	37278^{+875}_{-901}	31594^{+7788}_{-6863}	41726^{+1230}_{-1463}
$\log(g_{obs})$ /cm s^{-1}	(3)	3.73 ± 0.09	3.10 ± 0.06	4.25 ± 0.17	4.04 ± 0.40	4.05 ± 0.14
$\log(g_{rep})$ /cm s^{-1}	(4)	$3.77^{+0.08}_{-0.10}$	$3.10^{+0.07}_{-0.06}$	$4.14^{+0.08}_{-0.05}$	$4.15^{+0.11}_{-0.18}$	$4.12^{+0.06}_{-0.11}$
$vsin(i)_{obs}$ / km s^{-1}	(5)	204 ± 10	150 ± 28	230 ± 14	131 ± 28	273 ± 19
$vsin(i)_{rep}$ / km s^{-1}	(6)	200^{+16}_{-7}	150^{+28}_{-29}	230^{+15}_{-16}	130^{+28}_{-29}	270^{+23}_{-16}
$M_{1,act}$	(7)	$18.4^{+1.6}_{-1.4}$	$33.2^{+7.7}_{-3.5}$	$25.5^{+2.5}_{-1.7}$	$13.4^{+12.1}_{-7.1}$	$36.6^{+5.0}_{-5.5}$
$M_{1,ini}$	(8)	$18.6^{+1.7}_{-1.4}$	$38.0^{+7.7}_{-6.3}$	$25.6^{+2.6}_{-1.8}$	$13.4^{+12.3}_{-7.3}$	$37.2^{+5.5}_{-5.6}$
$R / R_\odot$	(9)	$9.3^{+1.5}_{-1.3}$	$26.7^{+4.4}_{-3.3}$	$7.1^{+0.7}_{-0.7}$	$5.9^{+2.6}_{-2.3}$	$8.5^{+1.7}_{-0.8}$
Age /Myr	(10)	$6.16^{+0.32}_{-0.32}$	$3.94^{+0.67}_{-0.67}$	$0.02^{+1.81}_{-0.01}$	$1.49^{+3.48}_{-1.50}$	$1.54^{+0.62}_{-1.30}$

system	spect. type	$M_{1,act}$ /$M_\odot$	$M_{1,ini}$ /$M_\odot$	$T_{eff,obs}$ /K	$\log(L_{obs}/L_\odot)$	$T_{eff,rep}$ /K	$\log(L_{rep}/L_\odot)$	R $R_\odot$	Age Myr
(1)	(2)	(3)	(4)	(5)	(6)	(7)	(8)	(9)	(10)
064[b]	O7.5 II(f)	48.2	51.8	35500	5.86	35469	5.82	22.2	2.94
073	O9.5 III	20.0	20.4	31800	4.99	31820	4.95	9.7	5.72
086	O9 III((n))	35.8	37.8	32800	5.62	32806	5.57	18.2	3.76
093	O9.2 III-IV	22.0	21.0	32300	5.01	32325	4.96	9.6	5.48
171	O8 II-III(f)	31.8	32.8	34600	5.48	34617	5.45	14.5	3.74
184	O6.5 Vnz	26.6	26.8	38900	5.07	38931	4.99	6.8	2.30
191	O9.5 V	18.6	18.4	32900	4.78	32891	4.74	7.2	5.18
243	O7 V(n)((f))	30.8	31.0	37900	5.36	37886	5.32	10.6	3.26
256	O7.5-8 V((n))z	23.2	23.4	36900	4.99	36911	4.85	6.5	3.28
277	O9 V	21.4	21.6	33900	5.00	33889	4.96	8.7	4.78
332[b]	O9.2 II-III	27.2	27.8	32100	5.35	32093	5.32	14.9	4.82
333[b]	O8 II-III((f))	51.4	56.6	34600	5.93	34612	5.86	23.1	2.74
404	O3.5 V(n)((fc))	39.0	39.6	43900	5.49	43922	5.36	8.2	1.72
409	O4 V((f))z	56.0	59.8	44900	5.90	44922	5.87	13.4	1.66
429	O7.5-8 V	27.8	27.2	36900	5.22	36911	5.18	9.4	3.60
440[b]	O6-6.5 II(f)	49.8	51.8	38500	5.85	38542	5.79	17.6	2.60
441	O9.5 V	20.0	20.2	32900	4.93	32931	4.89	8.6	5.22
479	O4-5 V((fc))z	35.2	35.4	42900	5.24	42886	5.26	7.8	0.60
481	O8.5 III	28.0	29.4	33900	5.37	33911	5.34	13.2	4.38
532	O3 V(n)((f*))z + OB	52.8	54.8	45900	5.80	45923	5.75	11.6	1.48
603	O4 III(fc)	65.0	69.4	43400	6.03	43390	5.99	18.0	1.84
613	O8.5 Vz	21.0	21.4	34900	4.95	34935	4.91	7.8	4.32
619	O7-8 V(n)	23.0	23.0	36900	4.91	36931	4.85	5.9	3.56
631	O9.7 III(n)	16.2	16.4	30400	4.66	30413	4.63	7.2	7.16
645	O9.5 V((n))	17.8	17.8	32900	4.70	32911	4.56	6.0	5.00
657	O7-8 II(f)	37.2	39.6	35500	5.65	35485	5.62	16.5	3.30
702	O8 V(n)	24.6	24.8	35900	5.13	35889	5.09	9.2	3.96
736	O9.5 V	18.6	18.8	32900	4.81	32891	4.76	7.3	5.18
743	O9.5 V((n))	18.6	18.4	32900	4.78	32981	4.74	7.2	5.18
750[b]	O9.5 IV	17.2	17.2	32300	4.67	32334	4.62	6.5	5.38
769	O9.7 II-III	17.0	16.6	29500	4.75	29500	4.72	8.6	7.24
802	O7.5 Vz	27.8	27.4	36900	5.23	36911	5.18	9.6	3.60
812	O4-5 V((fc))	40.8	41.8	42900	5.58	42879	5.55	10.7	2.04

Table A.4: physical quantities of the SB1-systems, especially the derived lower and upper mass-limits

system[a] [b]	spect. type	M_1	P[c]	K_1	e	$f(m)$	$M_{2,min}$	q_{min}	f_2/f_1	Δm	$q(f_2/f_1 = 0.1)$	$q(f_2/f_1\ q = 0.2)$	$q(f_2/f_1 = 0.3)$	$M_{2,min,ini}$	$q_{min,ini}$
		$M_\odot$	*days*	kms^{-1}		$/M_\odot$	$/M_\odot$			(f_2/f_1)/mag				$/M_\odot$	
(1)	(2)	(3)	(4)	(5)	(6)	(7)	(8)	(9)	(10)	(11)	(12)	(13)	(14)	(15)	(16)
HDE 308813	B0 V	18.4	6.34	22.2	0.0	0.007 ± 0.001	1.4	0.08	0.002	6.73	0.26	0.37	0.47	29.9	1.61
HD 152147	O9.5 I	33.2	13.82	13.1	0.0	0.003 ± 0.001	1.6	0.05	0.002	7.04	0.23	0.34	0.43	49.8	1.31
HD 164536	O6.5 V	25.4	13.4	26.2	0.0	0.025 ± 0.004	2.7	0.11	0.01	4.81	0.28	0.41	0.51		
BD-16°4826	O5.5 V	11.6	15.8	13.1	0.0	0.004 ± 0.001	0.9	0.07	0.00009	10.16	0.36	0.52	0.65	263.5	19.66
HDE 229232	O5 V	36.6	6.2	15.6	0.0	0.002 ± 0.001	1.5	0.04	0.0005	8.32	0.28	0.42	0.53	243.7	6.55
064[b]	O7.5 II(f)	48.2	902.9	57.2	0.53	10.74 ± 0.34	44.7	0.93	0.97	0.03	0.26	0.38	0.48	74.3	1.43
073	O9.5 III	20.0	150.60	27.0	0.20	0.29 ± 0.02	5.8	0.29	0.11	2.38	0.27	0.38	0.48	32.3	1.58
086	O9 III((n))	35.8	182.95	12.9	0.51	0.026 ± 0.003	3.4	0.10	0.02	4.52	0.24	0.36	0.45	52.9	1.40
093	O9.2 III-IV	22.0	250.13	10.9	0.20	0.031 ± 0.002	2.7	0.12	0.02	4.50	0.25	0.36	0.45	33.8	1.61
120	O9.5 IV		15.65	24.7	0.28	0.022 ± 0.001									
171	O8 II-III(f)	31.8	677.00	11.8	0.56	0.066 ± 0.002	4.4	0.14	0.03	3.82	0.25	0.38	0.47	53.3	1.62
184	O6.5 Vnz	26.6	32.13	12.1	0.20	0.006 ± 0.002	1.6	0.06	0.001	7.22	0.28	0.42	0.53	109.7	4.09
191	O9.5 V	18.6	358.90	23.0	0.22	0.42 ± 0.13	6.4	0.34	0.14	2.11	0.27	0.40	0.50	36.0	1.96
201	O9.7 V + sec		15.33	50.6	0.46	0.14 ± 0.04									
225	B0.7-1III-II		8.23	29.2	0.02	0.021 ± 0.001									
231	O9.7 IV:(n) + sec		7.93	50.2	0.41	0.08 ± 0.01									
243	O7 V(n)((f))	30.8	10.40	82.8	0.02	0.61 ± 0.01	10.1	0.33	0.14	2.12	0.27	0.40	0.50		
243[a]	O7 V(n)((f))	30.8	10.40	83.3	0.0	0.62 ± 0.01	10.1	0.33	0.14	2.12	0.27	0.40	0.50	64.1	2.07
256	O7.5-8 V((n))z	23.2	246.00	19.2	0.63	0.085 ± 0.008	4.0	0.17	0.03	3.70	0.28	0.41	0.52	63.5	2.71
277	O9 V	21.4	240.42	63.6	0.93	0.33 ± 0.12	6.3	0.30	0.12	2.34	0.27	0.39	0.50	39.4	1.83
314	O9.7 IV:(n) + sec		2.55	110.8	0.17	0.34 ± 0.01									
318	O((n))p		14.00	23.3	0.08	0.018 ± 0.003									
318[a]	O((n))p		14.00	23.1	0.0	0.018 ± 0.003									
329	O9.7 II-III(n)		7.05	61.3	0.43	0.12 ± 0.01									
332[b]	O9.2 II-III	27.2	1025.30	48.2	0.81	2.34 ± 1.66	16.4	0.60	0.49	0.78	0.25	0.36	0.45	39.1	1.41
333[b]	O8 II-III((f))	51.4	980.10	26.0	0.75	0.53 ± 0.01	13.0	0.25	0.10	2.55	0.26	0.38	0.48	82.6	1.46
350	O8 V		69.57	60.2	0.35	1.29 ± 0.03									
386	O9 IV(n)		20.44	14.3	0.25	0.006 ± 0.006									
390	O5-6 V(n)((fc))z		21.91	69.7	0.50	0.50 ± 0.03									
404	O3.5 V(n)((fc))	39.0	145.76	27.3	0.72	0.10 ± 0.01	5.9	0.15	0.03	3.87	0.29	0.43	0.55	190.7	4.81
409	O4 V((f))z	56.0	22.19	43.2	0.29	0.162 ± 0.008	8.8	0.16	0.03	3.74	0.30	0.45	0.57	205.8	3.44

[a] Solutions obtained by keeping e = 0 and $\omega = 90°$

[b] Systems with $P_{orb} > 1$ yr which need confirmation due to intrinsic limitation in the time series by [10]

[c] more accurate data and error bars can be found in Williams, S.J. et al [9] and Almeida L.A. et al [10]

Table A.5: physical quantities of the SB1-systems, especially the derived lower and upper mass-limits

system [a] [b]	spect. type	M_1 $M_\odot$	P [c] $days$	K_1 kms^{-1}	e	$f(m)$ $/M_\odot$	$M_{2,min}$ $/M_\odot$	q_{min}	f_2/f_1	Δm (f_2/f_1)/mag	$q(f_2/f_1 = 0.1)$	$q(f_2/f_1 q = 0.2)$	$q(f_2/f_1 = 0.3)$	$M_{2,min,ini}$ $/M_\odot$	$q_{min,ini}$
(1)	(2)	(3)	(4)	(5)	(6)	(7)	(8)	(9)	(10)	(11)	(12)	(13)	(14)	(15)	(16)
429	O7.5-8 V	27.8	30.04	92.4	0.56	1.40 ± 0.34	13.3	0.48	0.29	1.35	0.26	0.39	0.49	56.0	2.06
440[b]	O6-6.5 II(f)	49.8	1019.10	11.7	0.28	0.15 ± 0.02	7.9	0.16	0.04	3.50	0.26	0.39	0.49	89.6	1.73
441	O9.5 V	20.0	6.87	65.7	0.22	0.19 ± 0.01	4.9	0.24	0.07	2.84	0.27	0.39	0.49	35.7	1.77
475	O9.7 III		4.05	63.9	0.57	0.06 ± 0.02									
479	O4-5 V((fc))z	35.2	14.73	73.0	0.31	0.51 ± 0.02	10.1	0.29	0.10	2.51	0.29	0.43	0.54	30920.5	873.46
481	O8.5 III	28.0	141.82	128.3	0.93	1.57 ± 0.20	14.0	0.50	0.32	1.25	0.26	0.38	0.48	43.7	1.49
514	O9.7 III		184.92	22.9	0.41	0.18 ± 0.01									
532	O3 V(n)((f*))z + OB	52.8	5.80	34.4	0.46	0.017 ± 0.002	3.8	0.07	0.006	5.58	0.30	0.45	0.56	267.8	4.89
603	O4 III(fc)	65.0	1.76	11.4	0.11	$3 \cdot 10^{-5} \pm 10^{-5}$	1.0	0.02	$3 \cdot 10^{-5}$	10.21	0.29	0.44	0.55	165.9	2.39
613	O8.5 Vz	21.0	69.16	32.0	0.35	0.19 ± 0.09	5.1	0.24	0.07	2.90	0.28	0.40	0.51	44.5	2.08
619	O7-8 V(n)	23.0	14.50	36.8	0.09	0.074 ± 0.008	3.8	0.16	0.03	3.86	0.28	0.41	0.52	56.8	2.47
619[a]	O7-8 V(n)	23.0	14.50	36.8	0.0	0.075 ± 0.009	3.8	0.16	0.03	3.86	0.28	0.41	0.52	56.8	2.47
631	O9.7 III(n)	16.2	5.37	48.6	0.01	0.064 ± 0.004	2.9	0.18	0.03	3.75	0.28	0.40	0.49	25.7	1.57
631[a]	O9.7 III(n)	16.2	5.37	48.7	0.0	0.064 ± 0.004	2.9	0.18	0.03	3.75	0.28	0.40	0.49	25.7	1.57
645	O9.5 V((n))	17.8	12.55	31.6	0.24	0.038 ± 0.009	2.5	0.14	0.02	4.49	0.28	0.40	0.51	37.5	2.10
657	O7-8 II(f)	37.2	63.47	44.6	0.48	0.39 ± 0.03	9.5	0.26	0.10	2.52	0.26	0.39	0.49	63.0	1.59
702	O8 V(n)	24.6	1.98	105.6	0.01	0.24 ± 0.02	6.1	0.25	0.08	2.72	0.27	0.40	0.50	49.5	2.00
702[a]	O8 V(n)	24.6	1.98	105.9	0.0	0.24 ± 0.02	6.1	0.25	0.08	2.72	0.27	0.40	0.50	49.5	2.00
733	O9.7p		5.92	64.9	0.002	0.168 ± 0.002									
733[a]	O9.7p		5.92	65.1	0.0	0.17 ± 0.003									
736	O9.5 V	18.6	68.80	24.6	0.09	0.105 ± 0.006	3.7	0.20	0.04	3.37	0.28	0.40	0.50	36.0	1.92
743	O9.5 V((n))	18.6	14.95	23.4	0.01	0.020 ± 0.001	2.0	0.11	0.01	5.28	0.27	0.40	0.50	36.0	1.96
743[a]	O9.5 V((n))	18.6	14.95	23.4	0.0	0.020 ± 0.001	2.0	0.11	0.01	5.28	0.27	0.40	0.50	36.0	1.96
750[b]	O9.5 IV	17.2	416.70	29.5	0.78	0.27 ± 0.04	5.1	0.30	0.11	2.43	0.28	0.40	0.50	34.5	2.01
769	O9.7 II-III	17.0	2.37	40.8	0.01	0.017 ± 0.001	1.8	0.11	0.007	5.35	0.26	0.37	0.46	25.4	1.53
769[a]	O9.7 II-III	17.0	2.37	40.8	0.0	0.017 ± 0.001	1.8	0.11	0.007	5.35	0.26	0.37	0.46	25.4	1.53
779	B1 II-Ib		59.95	30.8	0.05	0.181 ± 0.004									
802	O7.5 Vz	27.8	181.88	58.5	0.60	0.92 ± 0.05	15.2	0.55	0.36	1.10	0.26	0.39	0.49	56.0	2.04
810	O9.7 V + B1:V:		15.69	100.7	0.68	0.66 ± 0.04									
812	O4-5 V((fc))	40.8	17.28	42.7	0.62	0.066 ± 0.003	5.2	0.13	0.02	4.14	0.29	0.43	0.54	135.9	3.25
827	B1.5 Ib		43.22	25.3	0.24	0.066 ± 0.003									
829	B1.5-2 II		202.93	12.6	0.27	0.037 ± 0.006									
887	O9.5 II-IIIn		2.67	30.07	0.06	0.008 ± 0.001									

[a] Solutions obtained by keeping e = 0 and $\omega = 90°$

[b] Systems with $P_{orb} > 1$ yr which need confirmation due to intrinsic limitation in the time series by [10]

[c] more accurate data and error bars can be found in Williams, S.J. et al [9]

List of Figures

List of Tables